EPiC Series in Technology
Volume 4, 2026, Pages 130–137
Proceedings of The 11th International Conference on Tribology in Manufacturing Processes & Advanced Surface Engineering

Influence of Asymmetric Plastic Flow and Tribological Conditions on Residual Stress and Dimensional Stability in Cold-Drawn AA3003-F Tubes

Norasak Sikkha[1,*], Numpon Mahayotsanun[2], Peerawatt Nunthavarawong[2], Pongsak Tuengsook[3] and Sedthawatt Sucharitpwatskul[4]
[1]Alumet Co., Ltd.
[2]King Mongkut's University of Technology North Bangkok
[3]King Mongkut's University of Technology Thonburi
[4]National Metal and Materials Technology Center
*noei.norasak@gmail.com

Abstract

Dimensional stability and interfacial friction remain critical challenges in precision aluminum tube manufacturing. This research investigates the influence of asymmetric plastic flow and tribological conditions on cold-drawn AA3003-F tubes through a systematic experimental investigation (N=30). Preliminary physical trials revealed that unlubricated drawing causes immediate tensile fracture at the tube head due to extreme interfacial friction, whereas the drawing process is successfully stabilized under a steady-state boundary lubricant ($\mu = 0.099$). During drawing, an initial eccentricity (2.34%–7.89%) acts as a catalyst, triggering a three-dimensional tilt of the cantilevered mandrel head under asymmetric drawing loads. This induces a highly unbalanced macro-residual stress distribution (ranging from -6 to -45 MPa as quantified via X-ray diffraction), where compressive residual stresses systematically concentrate in the thicker wall sectors. Mechanistically, this circumferential disparity drives inhomogeneous elastic recovery, generating an internal residual bending moment (M_{RS}) that severely deteriorates the longitudinal straightness from 1.080±0.669 mm/m to 2.973±0.942 mm/m. Concurrently, the ultimate tensile strength (UTS) increased from 140.26 ± 1.55 MPa to 151.11 ± 1.70 MPa, while ductility dropped severely, with elongation plummeting from 22.00% to 9.13% as the material reached its plastic instability limit. Crucially, the circumferential uniformity of Vickers hardness (44–45 HV) and stabilized X-ray line profile Full Width at Half Maximum (FWHM of 1.76–1.83 deg) confirm that the bowing defect is a macroscopic structural phenomenon arising from tool-workpiece mechanics rather than localized material defects. These findings emphasize the critical need for stringent initial

geometry control, alongside the use of fully-constrained tooling systems and optimized lubrication, to ensure the longitudinal accuracy of the final component.

1 Introduction

The manufacturing of precision thin-walled aluminum tubes primarily begins with the extrusion process (Sheppard, 1999), which defines the initial microstructural and geometric baseline of the AA3003-F state. While subsequent cold drawing improves mechanical properties and dimensional tolerance, a critical challenge arises from the transition from theoretical symmetry to real-world asymmetric loading. Industrial operations often suffer from improper mandrel adjustment, introducing an initial geometric eccentricity—ranging from 2.34% to 7.89% in AA3003-F tubes (Tang & Chatti, 2013). This geometric irregularity dictates a thickness variance between the thin wall (t_{thin}) and the thick wall (t_{thick}), acting as a catalyst for non-homogeneous plastic deformation and initiating a plastic strain gradient ($\partial\epsilon/\partial x$).

Such structural asymmetry necessitates the accumulation of Geometrically Necessary Dislocations (GNDs) to maintain lattice compatibility, ultimately driving localized work hardening. Despite achieving a stabilized equivalent hardness, the resulting asymmetric macro-residual stresses generate a residual bending moment (M_{RS}) that compromises the straightness of the final component. Therefore, this study systematically investigates the influence of initial geometric eccentricity and asymmetric plastic flow on the microstructural evolution, macroscopic properties, and dimensional precision of cold-drawn AA3003-F tubes using systematic experimental characterization, high-resolution X-ray diffraction, and advanced tribological testing.

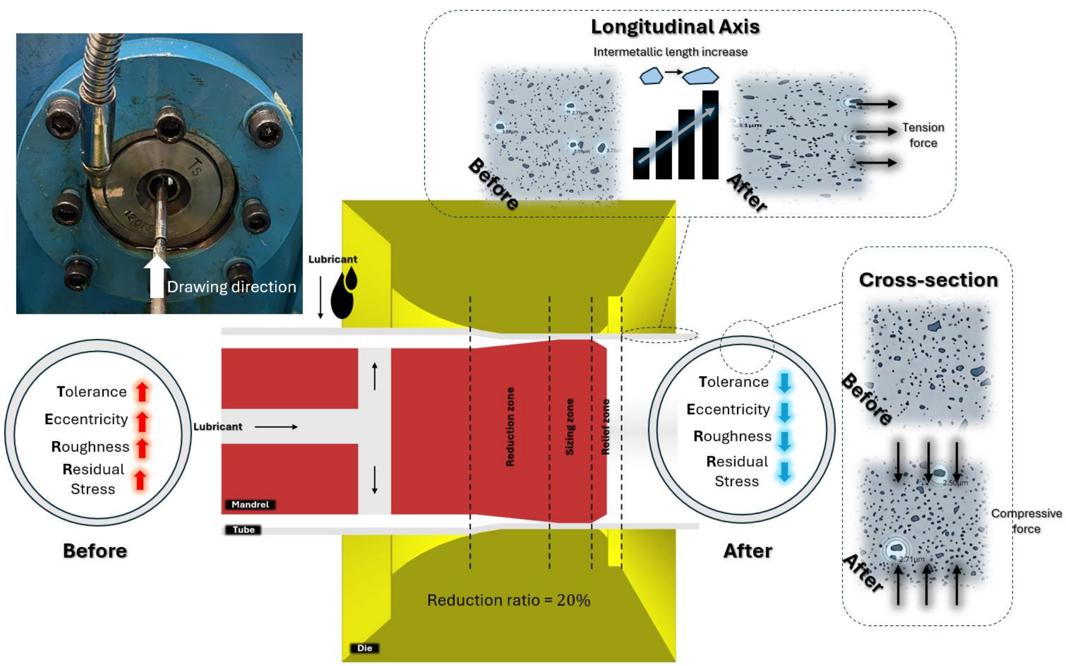

Figure 1: Schematic representation of microstructural evolution and geometric refinements during the cold drawing of AA3003-F tubes

2 Initial Geometry and Mechanics of Bowing Deflection

An evaluation of 30 as-extruded AA3003-F specimens (OD = 26.226 ± 0.031 mm) revealed a highly non-uniform circumferential wall thickness. The minimum thickness (t_{thin}) consistently localized at the 0°–45° sectors (0.894 ± 0.043 mm), while the maximum thickness (t_{thick}) shifted to the 135°–180° sectors (0.962 ± 0.045 mm). This circumferential wall thickness variation induced a significant initial eccentricity (2.34%–7.89%), acting as the primary catalyst for highly asymmetric plastic flow and the subsequent development of unbalanced residual stress states.

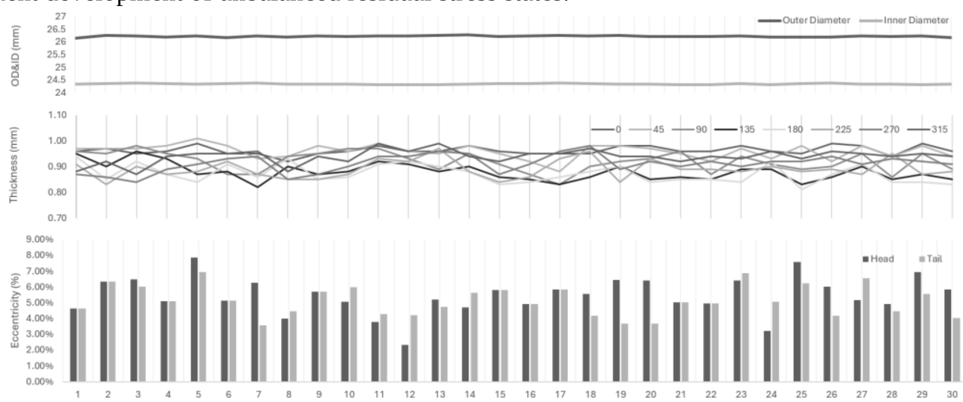

Figure 2: Initial geometric profiles, circumferential wall thickness variations, and eccentricity percentages of as-received AA3003-F tubes across 30 specimens.

During cold drawing, this thickness variance dictates that the thicker and thinner sectors experience differing levels of plastic strain and contact pressure at the tool-workpiece interface. Upon unloading, the magnitude of elastic springback varies significantly across the tube circumference, a phenomenon termed *inhomogeneous elastic recovery*. This generates an unbalanced axial residual stress (σ_{RS}) distribution, creating a resultant internal residual bending moment (M_{RS}) relative to the neutral axis (y) over the differential cross-sectional area (dA) (Dieter, 1986):

$$M_{RS} = \int_A \sigma_{RS} \cdot y dA \tag{1}$$

Based on the classical elastic curve theory (Totten et al., 2002), this internal residual moment (M_{RS}) serves as the primary driver for the longitudinal bowing defect (δ) over the tube length (L), given the tube's area moment of inertia (I) and Young's modulus (E) :

$$\delta = \frac{M_{RS} \cdot L^2}{8E \cdot I} \tag{2}$$

3 Experimental and Analytical Methodology

The study utilized 30 specimens of commercially extruded AA3003-F tubes (2.6 m length).

Element	Al	Mn	Fe	Cu	Si	Zn
Wt.%	Bal.	1.320	0.198	0.074	0.297	0.015

Table 1: Chemical composition of the AA3003-F aluminum alloy

To ensure process viability and accurately define interfacial conditions, a Twist Compression Test (TCT) was conducted, confirming a stable boundary friction coefficient (μ) of 0.099 (Gludovatz & Ritchie, 2016).

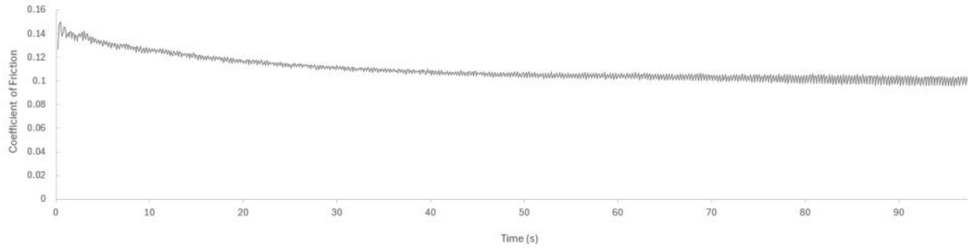

Figure 3: Tribological behavior of the lubricant showing the transition to a steady-state friction coefficient of 0.099, confirming boundary film stability.

The drawing operation employed a cantilevered fixed-mandrel setup configured for a 20% area reduction. Tensile testing was systematically performed to establish the mechanical baseline of the as-received tubes, yielding a True Ultimate Tensile Strength (UTS) of 169 MPa. Post-drawing, microstructural evolution was evaluated via optical microscopy. To systematically characterize the induced post-drawing stress states and structural uniformity across the tube circumference, macro-residual stresses and Full Width at Half Maximum (FWHM) profiles were quantified using a Pulstec μ-X360s X-ray diffractometer.

4 Results and Discussion

4.1 Microstructural Transformation

Asymmetric plastic flow is permanently recorded within the resulting grain morphology. Following the cold drawing process, randomly distributed intermetallic particles became highly aligned and elongated to lengths along the drawing axis (Babaghorbani et al., 2010). This microstructural compaction triggers severe forest dislocation entanglement, which effectively pins dislocations and induces the observed mechanical saturation across the tube's circumference.

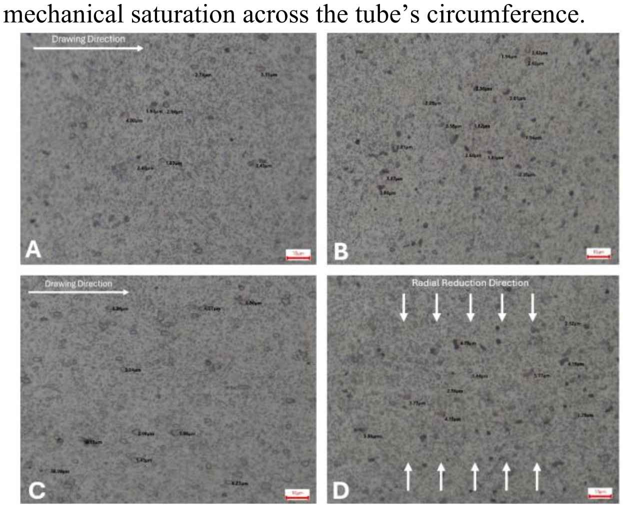

Figure 4: Microstructural evolution showing (A, C) longitudinal particle elongation and (B, D) increased cross-sectional spatial density

To maintain lattice compatibility under the asymmetric plastic strain gradient ($\partial \varepsilon / \partial x$) induced by the initial geometric eccentricity, the material develops a network of geometrically necessary dislocations (GNDs). The density of this GND network (ρ_{GND}) is directly proportional to Nye's factor (f) and inversely proportional to the Burgers vector (b) according to the following relation:

$$\rho_{GND} = f \cdot \frac{1}{b} \cdot \frac{\partial \epsilon}{\partial x} \tag{3}$$

4.2 Strengthening Mechanisms and the Ductility Drop

The cold drawing process significantly enhanced the overall material strength, with the yield strength rising to 65.00 ± 4.08 and the ultimate tensile strength (UTS) increasing from 140.26 ± 1.55 MPa to 151.11 ± 1.70 MPa. Concurrently, the Vickers hardness stabilized uniformly across the entire tube circumference within a narrow range of 44–45 HV.

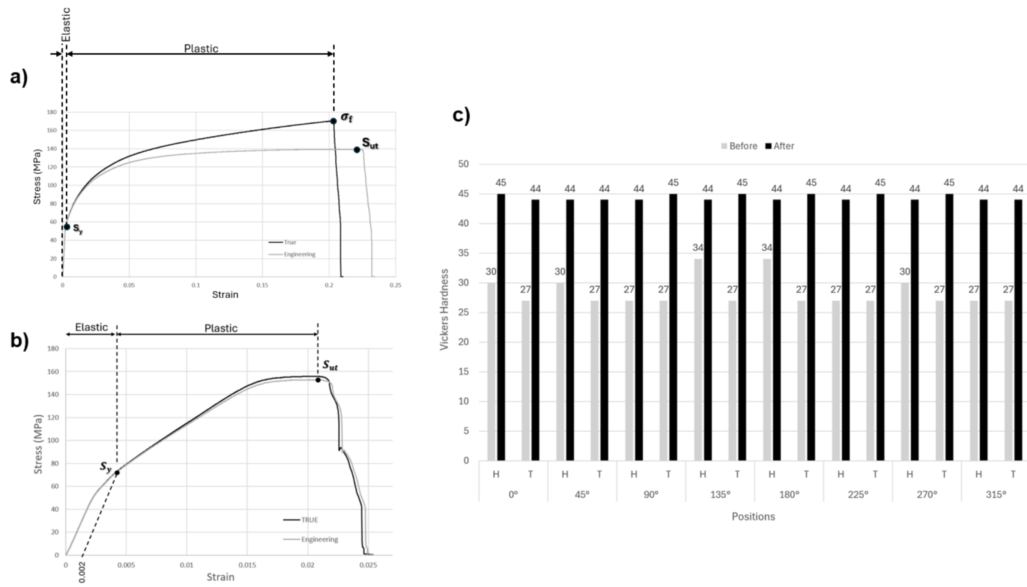

Figure 5: Mechanical property characterization of AA3003-F tubes: (a) Stress-strain curves in the as-extruded state (b) Stress-strain curves post-cold drawing and (c) Comparison of equivalent Vickers hardness across the circumference

However, this strengthening was accompanied by a severe ductility drop, with the total engineering elongation plummeting from 22.00% to 9.13%. In this deformed state, the strain-hardening exponent () approaches zero, signaling a state of mechanical saturation. At this saturation limit, the exceptionally high density of accumulated dislocations severely restricts further dislocation multiplication and mobility, thereby escalating the risk of premature fracture during subsequent secondary forming operations (Totten et al., 2002).

4.3 Macro-Residual Stress and FWHM Analysis

Experimental X-ray diffraction (XRD) characterization revealed a highly non-uniform macro-residual stress distribution across the drawn tube circumference, reflecting the direct physical consequence of asymmetric plastic flow. Post-drawing macro-residual stresses were predominantly compressive, quantified between -6 and -45 MPa, representing a significant escalation from the as-extruded baseline (Lobry et al., 2011). The peak longitudinal compressive stress systematically localized at the Top-Left (TL) sector, whereas the maximum hoop compressive stress concentrated at the Bottom-Right (BR) sector.

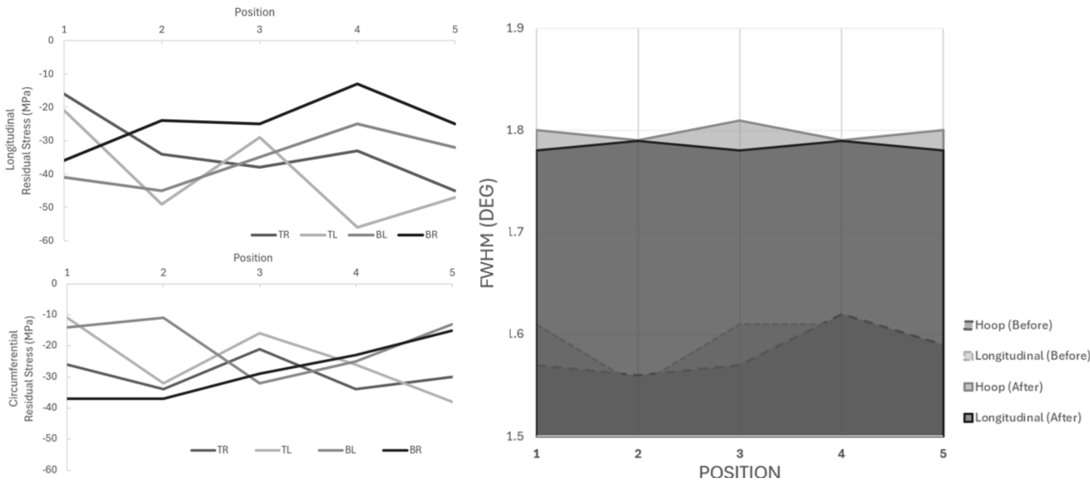

Figure 6: Asymmetric distribution of macro-residual stresses (XRD) and stable FWHM values across the tube circumference

This axis-dependent localization is physically driven by the three-dimensional tool misalignment (specifically, the cantilevered mandrel head tilt) that occurs under asymmetric drawing loads. Furthermore, the X-ray line profile Full Width at Half Maximum (FWHM) values stabilized uniformly within a narrow range of 1.76 –1.83 deg across all circumferential positions, reinforcing that the overall dislocation density reached a dynamic recovery equilibrium during the cold drawing process.

4.4 Geometric Integrity and Tribological Performance

The drawing process achieved precise control over the tube's cross-sectional geometry, yielding a 57. 50% improvement in eccentricity and a 59.55% reduction in roundness deviation. Surface roughness also exhibited significant improvements, with the arithmetic mean roughness (R_a) decreasing by 21.50%, and the ten-point mean roughness (R_z) by 18.17%. These surface refinements empirically confirm the high efficacy of the applied boundary lubricant ($\mu = 0.099$) in maintaining a continuous and stable tribological film, which successfully prevented catastrophic metal-to-metal contact under high contact pressures

Parameter	Unit	Before Drawing	After Drawing	Improvement (%)
Outer Diameter	*mm*	26.234 ± 0.033	24.707 ± 0.011	-
Wall Thickness	*mm*	0.919 ± 0.020	0.702 ± 0.014	-
Roundness	*%*	5.39 ± 1.19	2.18 ± 0.66	59.55
Eccentricity	*mm*	0.120 ± 0.071	0.051 ± 0.037	57.50
Dimensional taper	*mm/m*	-	0.010 ± 0.010	-
Roughness [R_a]	μm	0.507 ± 0.204	0.398 ± 0.182	21.50
Roughness [R_z]	μm	2.564 ± 0.846	2.098 ± 0.776	18.17
Straightness	*mm/m*	1.080 ± 0.669	2.973 ± 0.942	-

Table 2: Comparison of geometric accuracy and dimensional improvements of AA3003-F tubes before and after the cold drawing process

However, a significant longitudinal straightness paradox emerged; the straightness deviation substantially deteriorated from 1.080±0.669 mm/m to 2.973±0.942 mm/m. The inherited initial geometric eccentricity (2.34%–7.89%) acts as the fundamental driver of this instability. During deformation, it triggers asymmetric plastic flow and subsequent inhomogeneous elastic recovery upon unloading, thereby generating the internal residual bending moment (M_{RS}) that forces the tube to bow along its length.

5 Conclusions and Recommendations

5.1 Conclusions

This study establishes that the dimensional stability of cold-drawn AA3003-F aluminum tubes is fundamentally governed by both tribological conditions and initial geometric irregularities. The critical findings of this research are summarized as follows:

- Tribological Impact and Fracture Prevention: Preliminary physical trials demonstrated that unlubricated drawing causes immediate tensile fracture at the tube head due to extreme interfacial friction. In contrast, the application of a stable boundary lubricant ($\mu = 0.099$) successfully prevents metal-to-metal contact and mitigates interfacial friction-induced loading. This tribological control ensures process viability under severe plastic deformation by preventing interfacial stresses from breaching the material's fracture limit.

- Geometric Refinement and Mechanical Saturation: During drawing, the initial eccentricity (2.34%–7.89%) acts as the primary catalyst for asymmetric plastic flow. Although this flow successfully improved cross-sectional roundness by 59.55% and eccentricity by 57.50%, it drove the material to uniform mechanical saturation. This is empirically evidenced by stabilized FWHM values (1.76–1.83 deg) and consistent Vickers hardness (44–45 HV) across the entire cross-section.
- Inhomogeneous Elastic Recovery and Bowing: Unbalanced drawing loads cause the cantilevered mandrel head to tilt, resulting in an asymmetric macro-residual stress distribution (−6 to −45 MPa as quantified via X-ray diffraction), where higher compressive stresses systematically concentrate in the thicker wall sectors. Mechanistically, this localized disparity causes inhomogeneous elastic recovery upon unloading, generating an unbalanced internal residual bending moment (M_{RS}). According to classical Elastic Curve theory, this internal moment acts as the primary driver of the longitudinal bowing defect, permanently compromising longitudinal straightness despite cross-sectional improvements.
- The Mechanical Paradox (Strength vs. Ductility): The process effectively enhanced the overall UTS from 140.26±1.55 MPa to 151.11±1.70 MPa, but simultaneously triggered a severe ductility drop, with elongation decreasing significantly from 22.00% to 9.13%. This reduction indicates that the material has reached its plastic instability limit as the strain-hardening exponent (n) approaches zero, rendering the final components highly susceptible to premature fracture during subsequent forming operations.

5.2 Recommendations

To ensure process viability and precision, this study strongly recommends the following industrial implementations:

- Upstream Extrusion & Tribological Control: Strictly control wall thickness eccentricity at the upstream extrusion stage by ensuring precise alignment of the extrusion die and mandrel. Concurrently, optimize boundary lubrication to prevent premature tensile fractures under severe drawing pressures.
- Advanced Tooling Redesign: Transitioning from conventional cantilevered setups to fully-constrained mandrel systems is strongly recommended to eliminate three-dimensional tool tilting and asymmetric plastic flow.
- Elimination of Manual Compensation: Relying on manual tool adjustments merely masks the internal energy imbalances (M_{RS}) rather than resolving them. This practice should be replaced by systematic tool alignment and targeted stress-relieving annealing to ensure both high ultimate strength and longitudinal straightness.

References

Babaghorbani, P., Poole, W. J., Wells, M. A., & Parson, N. C. (2010). The effect of cold deformation on annealing behavior of AA3xxx alloys. In *Proceedings of the 12th International Conference on Aluminium Alloys* (pp. 302-307).

Button, S. T. (2015). Guidelines for selecting plugs used in thin-walled tube drawing processes of metallic alloys. *Journal of Materials Research and Technology*, *4*, 154-161.

Dieter, G. E. (1986). *Mechanical metallurgy* (3rd ed.). McGraw-Hill.

Gludovatz, B., & Ritchie, R. O. (2016). Evidence of inverse Hall-Petch behavior and low friction and wear in high entropy alloys. *Advanced Materials*, *28*(39), 8620-8627.

Lobry, P., Błaż, L., Sugamata, M., & Kula, A. (2011). Effect of rapid solidification on structure and mechanical properties of Al-6Mn-3Mg alloy. *Archives of Materials Science and Engineering*, *49*(2), 97-102.

Palkowski, H., Brück, S., Pirling, T., & Carradò, A. (2013). Investigation on the residual stress state of drawn tubes by numerical simulation and neutron diffraction analysis. *Materials*, *6*(11), 5118-5131.

Sheppard, T. (1999). *Extrusion of aluminium alloys*. Kluwer Academic Publishers.

Tang, J., & Chatti, S. (2013). Advanced model for calculation of the neutral axis shifting and the wall thickness distribution in rotary draw bending processes. *International Journal of Mechanical Sciences*, *75*, 190-201.

Totten, G. E., Howes, M. A. H., & Inoue, T. (Eds.). (2002). *Handbook of residual stress and deformation*. ASM International.